Transmission-mode diamond white-beam position monitor at NSLS

Erik M. Muller,[a]* John Smedley,[b] Jen Bohon,[c] Xi Yang,[d] Mengjia Gaowei,[e] John Skinner,[f] Gianluigi De Geronimo,[b] Michael Sullivan,[c] Marc Allaire,[f] Jeffrey W. Keister,[d] Lonny Berman[d] and Annie Héroux[f]

[a]Physics and Astronomy Department, Stony Brook University, Stony Brook, NY 11794, USA, [b]Instrumentation Division, Brookhaven National Laboratory, Upton, NY 11973, USA, [c]Center for Synchrotron Biosciences, Case Western Reserve University, Upton, NY 11973, USA, [d]Photon Sciences, Brookhaven National Laboratory, Upton, NY 11973, USA, [e]Material Science and Engineering, Stony Brook University, Stony Brook, NY 11794, USA, and [f]Structural Biology Department, Brookhaven National Laboratory, Upton, NY 11973, USA.
E-mail: erik.muller@stonybrook.edu

Two transmission-mode diamond X-ray beam position monitors installed at National Synchrotron Light Source (NSLS) beamline X25 are described. Each diamond beam position monitor is constructed around two horizontally tiled electronic-grade (p.p.b. nitrogen impurity) single-crystal (001) CVD synthetic diamonds. The position, angle and flux of the white X-ray beam can be monitored in real time with a position resolution of 500 nm in the horizontal direction and 100 nm in the vertical direction for a 3 mm × 1 mm beam. The first diamond beam position monitor has been in operation in the white beam for more than one year without any observable degradation in performance. The installation of a second, more compact, diamond beam position monitor followed about six months later, adding the ability to measure the angular trajectory of the photon beam.

Keywords: diamond; detector; monitor; position-sensitive; quadrant; white beam; BPM; photon; undulator.

1. Introduction

Simultaneous monitoring of flux, position and timing of intense white beams from third- and fourth-generation light sources can provide an unprecedented tool for beamline and accelerator diagnostics. X-ray beam position monitors based on high-purity synthetic single-crystal diamonds have made great strides towards this goal (Bergonzo *et al.*, 2001; Bohon *et al.*, 2010; Morse *et al.*, 2010; Berdermann *et al.*, 2010). The flux measurements in such devices are linear over 12 orders of magnitude, from low-power monochromatic light to high-power focused white beams (Keister & Smedley, 2009; Bohon *et al.*, 2010). As opposed to position measurements by blades (Shu *et al.*, 1994), which only indicate the location of the beam center of mass based on the diffuse tails, a transmission-mode position monitor provides the location of the actual center of mass of the beam. This paper describes the design, construction and calibration of diamond white-beam position monitors (wBPMs) in the context of the National Synchrotron Light Source (NSLS) X25 beamline, as well as characterization of the correlated motion of the electron beam with the photon beam. The two wBPMs discussed are permanently installed and the flux, position and trajectory of the white beam are continuously monitored.

2. Beamline layout

The NSLS at Brookhaven National Laboratory operates at 2.8 GeV and a current up to 300 mA. Beamline X25 is a facility beamline dedicated to macromolecular crystallography and is part of a suite of beamlines operated by the PXRR group (Macromolecular Crystallography Research Resource group) and the NSLS. Over the past few years, major upgrades at the beamline have increased the available flux in order to enable use of smaller beams to match the progressively smaller size of samples brought to the beamline. Fig. 1 shows the layout of the X25 beamline. Prior to the installation of the wBPMs, the only beam diagnostic tools available were ionization gauges in the experimental hutch, downstream from all optical components. No device other than a fluorescent screen was available for the white beam, not only at X25 but at any beamline at the NSLS. Beamline X25 originally had a tungsten-blade beam position monitor (BPM) installed in the front-end which suffered an internal short circuit and is no longer in service. In addition, preliminary testing of a diamond-blade BPM for the Advanced Photon Source was carried out at X25 where our first wBPM is installed. The diamond-blade BPM has limited utility as it would have to block the user beam to have signal; this illustrates that blade-type BPMs are not appropriate
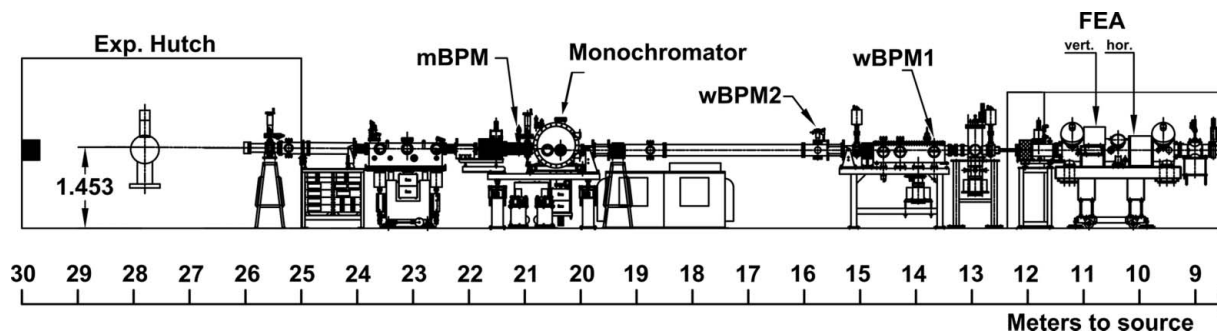
doi:10.1107/S0909049512005043 **381**

Figure 1
Layout of the NSLS X25 beamline highlighting the locations of the water-cooled upstream wBPM, compact downstream wBPM and the monochromatic mBPM. The undulator is not shown, but all distances are referenced to the center of the undulator position.

downstream of apertures. Being able to ascertain the quality of the incident beam on critical optical components such as the monochromator or focusing mirror is crucial in controlling the position stability of the beam at the sample.

An in-vacuum miniature gap undulator (Ablett & Berman, 2007) consisting of 18 mm periods (55 in total) can deliver 4.6×10^{11} photons s^{-1} across an energy range of 5 keV to 20 keV. This value is for experiments performed at 11.284 keV with a 100 µm × 100 µm aperture in the experimental hutch exposing the sample. A water-cooled aperture defines the size of the emitted photon beam. A thin graphite filter (295 µm thick) and a Be window (254 µm thick), attenuating only the low-energy photons, are the only optical elements between the source and the two wBPMs. These monitors are installed in the white beam at 13.5 m and 15.82 m from the center of the undulator source. The original blade-based BPM installed at the front-end was limited to qualitative measurements of the beam position because of stray low-energy radiation from a neighboring bending magnet (Berman et al., 1992). The diamond wBPMs are located after the Be window and graphite filter, and thus are not influenced by this radiation. Downstream of the second wBPM is a sagittally focusing silicon (111) double-crystal monochromator, followed by a commercial foil monochromatic beam position monitor (mBPM) and a focusing mirror, before entering the experimental hutch. The flux of the monochromatic beam is measured using ion chambers placed inside the hutch immediately after a Be window.

3. Mechanical design

The broad profile of the X25 undulator beam easily fills the maximum usable aperture size defined by the front-end apertures (FEAs) at 10 mm horizontally and 1 mm vertically. The FWHM of the full energy integrated beam at the position of the upstream diamond BPM is 8 mm horizontally and 2.4 mm vertically. At the time of development, there were no commercially available electronic-grade single-crystal diamonds large enough to accommodate the entire beam. To solve this problem, a novel design consisting of two horizontally tiled diamonds was employed to increase the overall width. Typically, a 3 mm × 1 mm white beam, defined by a water-cooled aperture, is used for crystallography experi-

ments, but a larger beam is sometimes required for experiments needing larger flux. The physical separation of the tiled diamonds is estimated to be approximately 50 µm.

Four 100 µm-thick electronic-grade single-crystal (001) synthetic chemical vapor deposition (CVD) diamonds from Diamond Detectors Ltd [grown by Element 6 (London, UK)] were selected from a batch of eight. They were screened using white-beam X-ray topography performed at NSLS X19C. Diamonds with the fewest defects known to cause photo-conductive gain in these devices (Muller et al., 2010) were selected. The diamond plates were then subjected to a standard chromic acid etching procedure to remove adventitious carbon from the surface. To supplement the oxygen surface termination left by the chromic acid etching procedure, the diamond plates were placed under an ultraviolet lamp in air for several hours. Platinum electrodes, 30 nm thick, were sputtered through a shadow mask in the pattern shown in Fig. 2(a); this thickness has proven to be sufficient for handling the current expected in these devices. Platinum contacts on oxygen-terminated diamond are known to greatly reduce hole injection into localized near-surface defects, suggestive of a blocking nature (Muller et al., 2010). Each diamond has two electrodes on the incident surface; the pair of diamonds completes the quadrant. The two wBPMs have different exit-side metalization geometry. On the upstream wBPM, each diamond has one solid 30 nm-thick platinum electrode with a total size matching that of the front two electrodes. The downstream detector has the same pattern of platinum electrodes on the exit side as the incident side.

Phosphor-bronze clamps hold the diamonds against a copper mount with a 1 mm overlap, providing both structural support and heat sinking. Electrical contact is made to the platinum pads using opposing phosphor-bronze clips. In the center of the device, the two diamond edges are placed in contact; the pad metalization is 200 µm from the edge of each diamond, making a total horizontal separation of ~400 µm. Two thermocouples (k-type) are used to monitor the temperature of the detector; one is placed just below the diamonds on the phosphor-bronze clamp and one several centimeters away on the copper housing. A copper mask is installed on the upstream wBPM, exposing only the diamonds and shielding the outer components while allowing a 3 mm path above the diamonds. The downstream wBPM includes a
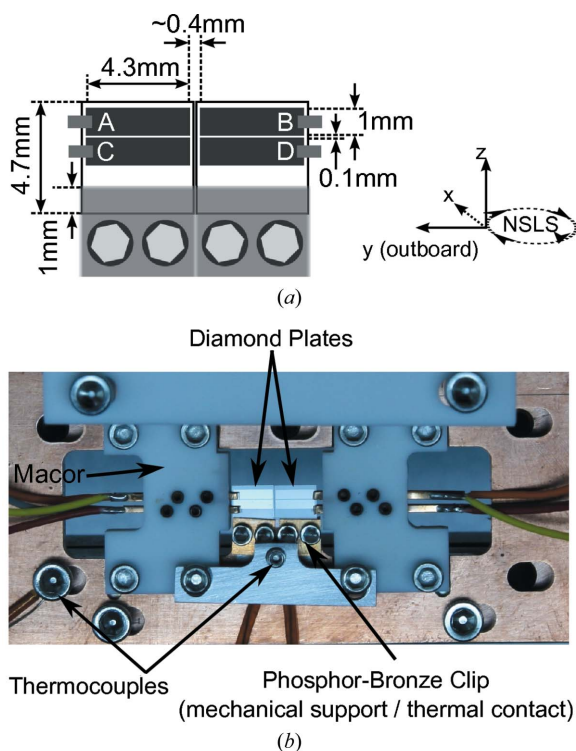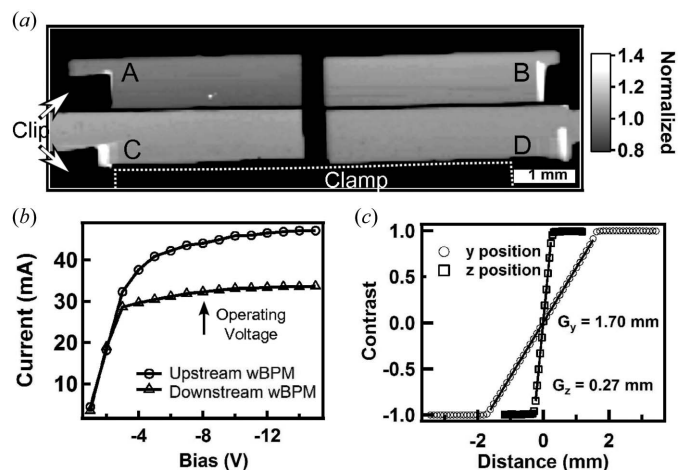
Figure 2
(a) Diagram of the electrical and thermal contacts to the diamonds as well as the dimensions of the platinum metalization. The overlap of the diamonds with the copper block is nominally 1 mm, clamped by a phosphor-bronze clip. (b) An overview photograph of the upstream water-cooled diamond wBPM, showing the intermediate electrical contacts and the Macor electrical isolation.

Figure 3
(a) XBIC image of the downstream diamond detector showing uniform response over the entire device (−50 V applied to the exit side of the diamond). The detector is rotated to avoid artifacts arising from the scan direction. The dark regions are caused by the electrical clips making contact with the platinum pads and by the phosphor-bronze clamp. The data are normalized to the expected value for full charge collection. (b) The sum of the current on the four pads *versus* the applied bias. The detectors are operated above the saturation region where there is full collection of the generated charge carriers. (c) Position calibration performed at beamline X28C.

similar mask, but made of molybdenum. The opening in the mask is ∼8 mm horizontally and ∼12 mm vertically, allowing a beam bypass above the diamonds similar to that for the upstream wBPM. The wBPMs have similar mounting near the diamonds, and are installed on a manipulator stage with horizontal and vertical motions for alignment. The upstream wBPM is mounted on a water-cooled copper block, making it bulky but very temperature stable. The downstream wBPM was designed for compactness, with no water cooling, instead relying on heat dissipation from the copper block and a copper rod support. The entire assembly for the second wBPM can fit through a standard 2.75 inch ConFlat flange.

4. Response uniformity and flux linearity

Prior to installation in the white beam, the electrical response in transmission mode for each diamond plate was characterized as described elsewhere (Keister & Smedley, 2009). It is important that the detector be free from regions of photoconductive gain to ensure predictable response dependent only on the absorbed X-ray flux. X-ray beam induced current (XBIC) mapping was performed at X25, where a 50 μm × 50 μm monochromatic beam (10 keV) was raster scanned across the plates (Fig. 3a). A 50 V bias was placed on the back electrode and the current was measured from each pad with Keithley electrometers (model numbers 6514 and 6517A). The data shown are from the upstream wBPM. The reduced

response in the unmetalized portion of the wBPM arises from the reduced electric field in this fringing region where full charge collection is not achieved. While some detrimental photoconductive gain was observed when using a positive bias, a uniform response with no photoconductive gain was exhibited in negative polarity.

During regular operation at the beamline, only negative bias is applied to back electrodes of the wBPMs, avoiding the photoconductive gain observed under positive bias. To minimize the ohmic heating in the devices, the lowest possible voltage is used while still remaining in saturation (at an operating voltage of 8 V, the measured charge collection efficiency is 96%) as shown in Fig. 3(b). The wBPMs were tested for flux linearity at NSLS X28C; see Fig. S1[1] (Bohon *et al.*, 2010), then calibrated at X25 to take into account the different incident beam sizes used. When both wBPMs are in use in the beam, the signal decreases by 33% on the downstream wBPM, as expected, owing to absorption of the low-energy photons by the first set of diamonds. The wBPMs absorb a significant fraction of the total X-ray power, but they do not significantly reduce the photons at energies where the beamline typically operates (11 keV to 13 keV). This is in agreement with theoretical values (CXRO) (Henke *et al.*, 1993), which predict that each device will reduce the number of relevant photons by only 5.4%.

The individual current for each quadrant is measured through a custom-built current-to-voltage amplifier capable of handing up to 3 A per channel. The voltage is read with an Acromag IP330 data acquisition board on an AVME 9668

---

[1] Supplementary data for this paper are available from the IUCr electronic archives (Reference: VV5032). Services for accessing these data are described at the back of the journal.

carrier card. The data are harvested continuously at the full bandwidth of the IP330 of 67 kHz and averaged into 1 Hz bins suitable for correlation with the experiments performed at the beamline. A flat data file is created with all the diagnostics values from the wBPMs, monochromatic BPM and ion gauges along the beamline. A plot is deposited in the experimental database showing the beam position and intensity for the users to correlate with their experimental data. The values are made available throughout the NSLS facility *via* an EPICS Channel Access gateway.

5. Thermal considerations

The temperature increase in the wBPM has two main contributions: X-ray power directly absorbed in the device and ohmic heating. The amount of X-ray power absorbed in the diamond depends on the energy spectrum of the undulator beam and the thickness of the diamond; fortunately, our results indicate that the temperature rise owing to absorption is negligible. The downstream wBPM temperature only drops a few degrees Kelvin when the X-rays are incident on them with the bias turned off; the temperature of the water-cooled upstream wBPM remains stable. Ohmic heating, however, places a significant heat load on the device. Again, this is why the wBPMs are operated at a low bias. After applying the nominal bias of 8 V, the upstream water-cooled wBPM, as expected, is very thermally stable and shows only slight, negligible motions with changing heat loads. The downstream wBPM, however, does have some noticeable motion with changing heat load (warm-up period after powering on the device). No change in temperature is observed when there is bias on the device but no incident light. This will be discussed in more detail in §7.

The front-end slits were opened completely to determine the maximum total optical flux (and power) in the white beam incident on the detectors. The horizontal extent of the beam is larger than the 8.0 mm horizontal aperture of the protective wBPM masks. The measurable vertical extent of the beam is limited by the total height of the active area on the plates (2 mm). With a synchrotron ring current of 265 mA and the undulator gap closed to 5.68 mm, fully illuminating the detector, total currents of 748 mA and 610 mA were observed in the upstream and downstream wBPMs, respectively. This corresponds to ∼80 W of total X-ray power incident on the first wBPM. The temperature at the diamond position under these conditions reached 384 K after several minutes of illumination.

6. Position calibration

The position of the X-ray beam is determined from the separation of charge carriers between the four quadrants of the wBPM, measured individually. The *y* and *z* positions of the beam are determined using the following formulae,

$$y = G_y \frac{(I_B + I_D) - (I_A + I_C)}{I_A + I_B + I_C + I_D}, \qquad (1)$$

$$z = G_z \frac{(I_A + I_B) - (I_B + I_D)}{I_A + I_B + I_C + I_D}, \qquad (2)$$

where *y* is defined as the horizontal outboard direction and *z* is the vertical direction. I_A, I_B, I_C and I_D are the currents collected from each of the four pads. G_y and G_z are the calibration constants in units of mm for a give beam size in the *y* and *z* directions, respectively.

The initial calibration, performed at X28C, was used to test the position and flux linearity, as well as thermal performance. Beamline X28C produces focused X-ray white beam capable of delivering almost 90 W mm^{-2} to the focal point (Sullivan *et al.*, 2008); however, full flux was not used in this test. A 4 mm × 1 mm aperture blocked the unfocused white beam to create a similar profile beam as that for X25. Each diamond detector was placed in a nitrogen enclosure to limit the ozone production by the X-ray beam which may degrade the electrodes. The devices were scanned through the beam in both the horizontal and vertical directions using precision motors. The sensitivity constants, G_y and G_z, were obtained from the inverse of the slope in the active region of the detector, as shown in Fig. 3(*c*). The sensitivity factors are unique for a specific beam shape and intensity profile. From this calibration graph, it can be determined that there is a large region over which the position calibration is linear, specifically, nearly 4 mm in the horizontal and 0.5 mm in the vertical dimensions.

7. Noise and stability

A measurement of the position noise was also performed at X25 on both wBPMs [Figs. 4(*a*) and 4(*b*)]. The two wBPMs are initially centered with respect to the beam; position and angle are measured with respect to this alignment. The r.m.s. noise, which includes all sources, is approximately 100 nm in the vertical direction and 500 nm in the horizontal. The comparatively high noise level in the horizontal is in part due to the beam shape (the beam is much wider than it is tall), and also to a decreased sensitivity in the detector owing to the separation of charge between two different diamonds. This effect can arise from geometrical and electrical asymmetries (defect density and thickness differences between the diamonds) near the inner edge of the diamond. Any slight asymmetry in the horizontal metalization can result in a situation where the charge generated in one diamond (and collected by that diamond) could be physically closer to the other diamond. This can result in an apparent motion in the opposite direction. Also, at the edge of the diamond where defect density is high, a non-uniform charge collection can have a similar effect. In Fig. 4(*b*) there is an apparent vertical thermal drift in the second uncooled wBPM of the order of 5 μm when the mini-gap undulator is closed to 5.6 mm, providing maximum flux. The apparent drift stabilizes over an hour, as the copper block support slowly heats to its equilibrium temperature of 318 K. The temperature near the
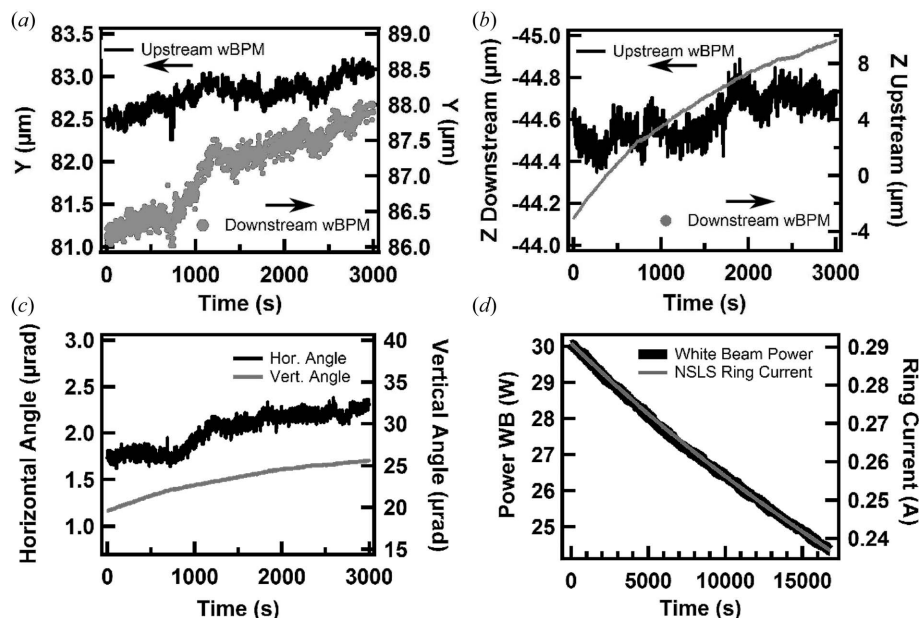
Figure 4
(a), (b) The horizontal and vertical position noise observed by both wBPMs. (c) The angular position of the photon beam. (d) Power in the white X-ray beam as measured by the wBPM and the current in the synchrotron storage ring.

diamonds reaches an equilibrium temperature of 325 K within a few minutes. Once the wBPM has stabilized, the vertical noise is comparable with that of the water-cooled upstream wBPM. This stabilization period induces an apparent drift of the vertical beam angle, stabilizing to a value of 0.07 µrad in the horizontal and 0.06 µrad in the vertical. The temperature of the two WBPMs also depends on the undulator gap. Fully closed (gap = 5.6 mm), the temperature nearest the diamond is 315 K and 349 K for the upsteam and downstream detectors, respectively. Fully open (gap = 7.0 mm), the temperature nearest the diamond is 313 K and 341 K for the upsteam and downstream detectors, respectively.

By taking the sums of the current in the four pads of each detector, the wBPMs can be used as flux monitors. With the known spectrum of the beamline undulator (Tanabe *et al.*, 2007), and the absorption in the diamond, the power in the white beam can be calculated. In Fig. 4(d) the white-beam power is overlayed with the current in the synchrotron storage ring. The power in the white beam was determined using the known undulator spectrum, the absorption of the diamond and the current in the device. The slow decay of the beam did not result in any change in the beam position, confirming the linearity of the response with incident power on the diamonds.

8. Motion of X-ray source

The wBPMs were used to investigate the correlation of the motion in the photon beam with motion of the electron beam as it passes through the undulator. In collaboration with the NSLS, the electron orbit was altered to provide local translations and angular changes in the electron beam. The beamline layout is crucial for understanding the motion observed by the two wBPMs. The position of the electron beam is monitored at both the entrance and exit of the undulator by pick-up electrodes (PUEs) which are capable of determining the position of the electron beam to a resolution of about 10 µm. From the undulator, the photon beam has a divergence of 0.4 mrad × 0.1 mrad (h × v), trimmed by front-end FEAs located 10 m downstream. The FEA defines a new virtual source for the two wBPMs and will impact the motion of the photon beam. The FEAs are normally set to 3 mm × 1 mm (h × v) but can be varied to accommodate some experiments.

The X25 beamline set-up results in parallax motion of the photon beam, pivoting about the FEA as the primary source moves, a real motion of the photon beam. This is best illustrated by making deliberate motions of the electron beam (Fig. 5a) and comparing these with the observed motions of the photon beam (Fig. 5b). The electron beam was moved in steps of 50 µm to a total vertical deviation from the standard orbit of 150 µm in both directions, recorded by the PUE on each side of the undulator. Upon deflection of the electron beam, the photon beam is observed to move in the opposite direction, which is consistent with parallax. As expected, the motion on the downstream wBPM is greater than on the upstream wBPM because the downstream wBPM is farther from the aperture than the upstream wBPM. The observed coupling between horizontal and vertical motions can arise from either a small angle between the detector orientation and the beam motion or a slight vertical misalignment between two diamonds of the same detector. A consequence of having the FEA is that a purely translational move of the electron beam introduces both a translation and an angular change to the photon beam. Unfortunately, the active area of the wBPM cannot accommodate the full undulator beam, so the aperture could not be removed or opened enough to avoid this effect.

The effects of angular motions of the electron beam on the photon beam were also investigated. Symmetrical movements of the electron beam (in opposite directions) about the center of the undulator were made, resulting in an angular trajectory of the electron beam through the undulator. We were limited to angles that were smaller than the source divergence (meaning that the aperture was still defining the beam size), thus only subtle movements in the photon beam were observed (Fig. 5c).

8.1. Undulator gap and photon beam motion

The beamline typically operates with the undulator gap between 5.6 mm and 7.0 mm. One of the first observations with the wBPM was that the photon beam, in some cases,
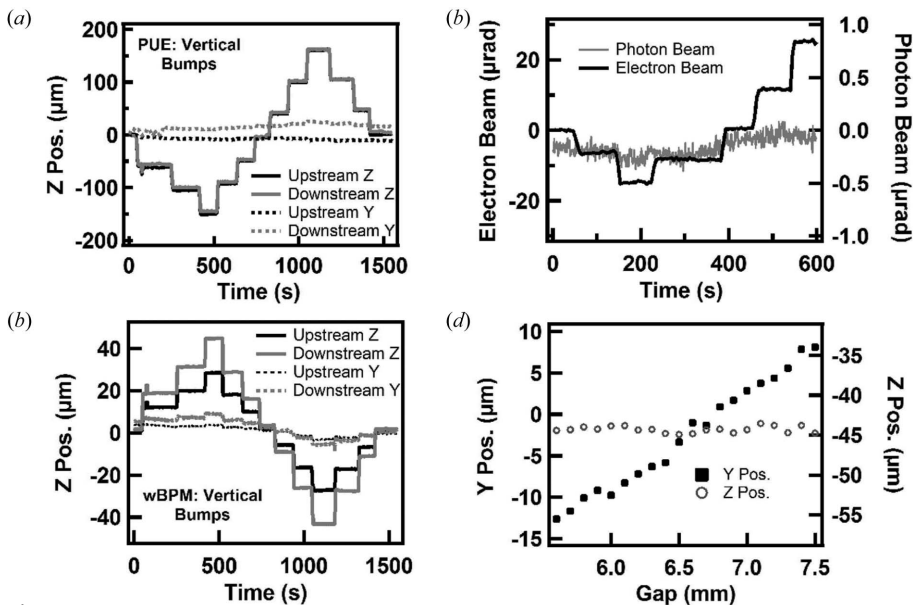
Figure 5
(a) Position of the electron beam showing 50 μm steps. (b) Corresponding motion of the photon beam as measured by both wBPMs. (c) Movement of the photon beam from angular movements of the electron beam, demonstrating that the photon beam does not respond to small angular motions of the electron beam. (d) Position dependence of the photon beam *versus* the undulator gap separation.

moves when the undulator gap is changed. It was also observed that intentional misalignment of the electron beam results in a photon beam position that depends on the value of the undulator gap. The stability of the photon beam position during undulator gap changes is dependent on both translation and angular movements of the electron beam. The horizontal position is most sensitive to the intentional misalignment, moving up to 15 μm as the gap is scanned from 5.6 mm to 7.0 mm for an intentional translational misalignment of 150 μm of the electron beam. In Fig. 5(d) the position of the photon beam is shown as a function of the undulator gap.

9. Conclusions

We have demonstrated that CVD diamond-based quadrant detectors perform well for constant monitoring of the flux and position of the white beam generated by an undulator. By employing two wBPMs, the angle of the photon beam can also be measured. The position sensitivity is 500 nm in the horizontal direction and 100 nm in the vertical direction for current devices. Up to 748 mA (gap of 5.68 mm) total current has been measured in the diamonds when the apertures were opened. A low bias is used to minimize the heat load on the device while still collecting all the generated charge carriers. Because of thermal drift in the non-water-cooled wBPM and the presence of the upstream FEAs, detection of angular motions of the beam are limited and should only be performed after they have thermally stabilized. The wBPM has proven to be reliable and robust, showing no degradation after more than one year in use. These devices represent a new type of beamline diagnostic, allowing inline optimization of the

undulator and calibration of the front-end apertures during commissioning of new beamlines as well as during normal operation. As they are sensitive to electron beam motion in the insertion device, they also represent an accelerator diagnostic to check and complement existing electron BPMs and could potentially be used to correct motions using a feed-forward procedure (Chrin *et al.*, 2008). The compact design allows easy installation in the beamline and the electronic readout set-up is simple and inexpensive to implement and incorporate into the beamline software.

References

Ablett, J. M. & Berman, L. E. (2007). *Nucl. Instrum. Methods Phys. Res. A*, **582**, 37–39.
Berdermann, E., Pomorski, M., de Boer, W., Ciobanu, M., Dunst, S., Grah, C., Ki, M., Koenig, W., Lange, W., Lohmann, W., Lovrincic, R., Moritz, P., Morse, J., Mueller, S., Pucci, A., Schreck, M., Rahman, S. & Traeger, M. (2010). *Diamond Relat. Mater.* **19**, 358–367.
Bergonzo, P., Tromson, D., Mer, C., Guizard, B., Foulon, F. & Brambilla, A. (2001). *Phys. Status Solidi A*, **185**, 167–181.
Berman, L. E., Hastings, J. B., Oversluizen, T. & Woodle, M. (1992). *Rev. Sci. Instrum.* **63**, 428–432.
Bohon, J., Muller, E. & Smedley, J. (2010). *J. Synchrotron Rad.* **17**, 711–718.
Chrin, J., Schmidt, A., Streun, A. & Zimoch, D. (2008). *Nucl. Instrum. Methods Phys. Res. A*, **592**, 141–153.

Henke, B. L., Gullikson, E. M. & Davis, J. C. (1993). *Atom. Data Nucl. Data Tables*, **54**, 181–342.

Keister, J. W. & Smedley, J. (2009). *Nucl. Instrum. Methods Phys. Res. A*, **606**, 774–779.

Morse, J., Solar, B. & Graafsma, H. (2010). *J. Synchrotron Rad.* **17**, 456–464.

Muller, E. M., Smedley, J., Raghothamachar, B., Gaowei, M., Keister, J. W., Ben-Zvi, I., Dudley, M. & Wu, Q. (2010). *Diamond Electronics and Bioelectronics Fundamentals to Applications III*, Vol. 1203, edited by P. Bergonzo, J. E. Butler, R. B. Jackman, K. P.

Loh and M. Nesladek, pp. J17–J19. Warrendale: Materials Research Society.

Shu, D., Collins, J. T., Barraza, J. & Kuzay, T. M. (1994). *Nucl. Instrum. Methods Phys. Res. A*, **347**, 577–580.

Sullivan, M. R., Rekhi, S., Bohon, J., Gupta, S., Abel, D., Toomey, J. & Chance, M. R. (2008). *Rev. Sci. Instrum.* **79**, 025101.

Tanabe, T., Ablett, J., Berman, L., Harder, D. A., Hulbert, S., Lehecka, M., Rakowsky, G., Skaritka, J., Deyhim, A., Johnson, E., Kulesza, J. & Waterman, D. (2007). *AIP Conf. Proc.* **879**, 283–286.